



Trafficking-defective mutant PROKR2 cycles between endoplasmic reticulum and Golgi to attenuate endoplasmic reticulum stress

Yong Bhum Song^{a,b}, Seung-Yeol Park^{c,d}, Kunyou Park^d, Hayoung Hwang^a, Rona S. Carroll^a, Victor W. Hsu^c, and Ursula B. Kaiser^{a,1}

^aDivision of Endocrinology, Diabetes and Hypertension, Brigham and Women's Hospital, Harvard Medical School, Boston, MA 02115; ^bDivision of Research Center, Scripps Korea Antibody Institute, Chuncheon 24341, Republic of Korea; ^cDivision of Rheumatology, Inflammation, and Immunity, Brigham and Women's Hospital, Harvard Medical School, Boston, MA 02115; and ^dDepartment of Life Sciences, Pohang University of Science and Technology (POSTECH), Pohang 37673, Republic of Korea

Edited by Robert Lefkowitz, HHMI, Durham, NC; received February 9, 2021; accepted December 10, 2021

G protein-coupled receptors (GPCRs) play crucial roles in numerous physiological and pathological processes. Mutations in GPCRs that result in loss of function or alterations in signaling can lead to inherited or acquired diseases. Herein, studying prokineticin receptor 2 (PROKR2), we initially identify distinct interactomes for wild-type (WT) versus a mutant (P290S) PROKR2 that causes hypogonadotropic hypogonadism. We then find that both the WT and mutant PROKR2 are targeted for endoplasmic reticulum (ER)-associated degradation, but the mutant is degraded to a greater extent. Further analysis revealed that both forms can also leave the ER to reach the Golgi. However, whereas most of the WT is further transported to the cell surface, most of the mutant is retrieved to the ER. Thus, the post-ER itinerary plays an important role in distinguishing the ultimate fate of the WT versus the mutant. We have further discovered that this post-ER itinerary reduces ER stress induced by the mutant PROKR2. Moreover, we extend the core findings to another model GPCR. Our findings advance the understanding of disease pathogenesis induced by a mutation at a key residue that is conserved across many GPCRs and thus contributes to a fundamental understanding of the diverse mechanisms used by cellular quality control to accommodate misfolded proteins.

Golgi | endoplasmic reticulum | PROKR2

G protein-coupled receptors (GPCRs), also known as seven transmembrane domain receptors, are the largest protein family encoded by the human genome. They serve many cellular functions and are the largest class of therapeutic drug targets (1–3). Mutations in GPCRs are being identified in many disease settings, including patients with neuroendocrine diseases (4). The understanding of abnormal phenotypes caused by these mutations has contributed to our knowledge of the pathophysiology of human diseases.

Several GPCRs, including gonadotropin-releasing hormone receptor (GnRHR), kisspeptin receptor, and tachykinin receptor 3, have roles in the reproductive neuroendocrine system. Mutations in these GPCRs lead to normosmic hypogonadotropic hypogonadism (HH) and Kallmann syndrome (KS), which are characterized by GnRH deficiency (5, 6). Prokineticin receptor 2 (PROKR2) and its ligand PROK2 have functional roles in multiple biological processes, including intestinal contraction, circadian rhythms, vascular and reproductive function, and the development of the olfactory system (7–13). *Prokr2*-deficient mice exhibit hypoplasia of the olfactory bulbs and abnormal migration of GnRH neurons as well as immature reproductive organs in both sexes (10). To date, over 20 missense mutations in the PROKR2 gene have been reported in patients with HH or KS (6, 14).

Human disorders associated with GPCR mutations—for example, retinitis pigmentosa, ovarian dysgenesis, and nephrogenic

diabetes as well as HH and KS—can occur as a result of defects in GPCR folding and trafficking (15). Over 50% of PROKR2 mutations identified in patients with HH and KS (11 of 21 mutations tested by functional assays) show impaired cell surface expression (6, 8, 16–19). Pharmacological chaperones have been used to rescue cell surface transport and function of some misfolded proteins, including GPCRs (20–22). For example, A457, an antagonist of PROKR2, has been used to restore cell surface expression and function of the P290S PROKR2 mutant, while treatment with 10% glycerol significantly increased cell surface expression and the signaling of P290S and W178S PROKR2 mutants (23). Thus, because cell surface expression is so critical for the function of many GPCRs, a better understanding of the different ways that mutations can alter the surface expression of GPCRs has been an important ongoing goal.

In the endoplasmic reticulum (ER), a quality control system ensures that only correctly folded proteins are transported out of this compartment, while misfolded proteins are targeted for degradation. Protein-folding chaperones in the ER such as BiP (also known as GRP78 or HSPA5) prevent protein aggregation by promoting the refolding of misfolded proteins. Exemplifying this role, studies have shown that misfolded mutant GPCRs

Significance

The endoplasmic reticulum (ER) possesses a quality control system that prevents misfolded proteins from leaving the ER for routing to the ER-associated degradation pathway. Some misfolded proteins can escape the ER to reach the Golgi, where they are then retrieved from the Golgi back to the ER for degradation, but why this occurs needs to be clarified. Studying a mutant prokineticin receptor 2 identified in patients with hypogonadotropic hypogonadism as a model, we find that the post-ER retrieval system provides another layer of quality control and also lowers the load of misfolded proteins in the ER to reduce ER stress. Our findings reveal the importance of a post-ER quality control mechanism in contributing to cellular homeostasis.

Author contributions: Y.B.S., R.S.C., V.W.H., and U.B.K. designed research; Y.B.S., S.-Y.P., K.P., H.H., and U.B.K. performed research; Y.B.S., S.-Y.P., K.P., V.W.H., and U.B.K. contributed new reagents/analytic tools; Y.B.S., R.S.C., V.W.H., and U.B.K. analyzed data; Y.B.S., R.S.C., V.W.H., and U.B.K. wrote the paper; and U.B.K. was involved in all aspects of research.

The authors declare no competing interest.

This article is a PNAS Direct Submission.

This article is distributed under [Creative Commons Attribution-NonCommercial-NoDerivatives License 4.0 \(CC BY-NC-ND\)](https://creativecommons.org/licenses/by-nc-nd/4.0/).

¹To whom correspondence may be addressed. Email: ukaiser@bwh.harvard.edu.

This article contains supporting information online at <http://www.pnas.org/lookup/suppl/doi:10.1073/pnas.2102248119/-DCSupplemental>.

Published February 16, 2022.

have increased association with ER chaperones compared to wild-type (WT) GPCRs (24–26). When refolding is unsuccessful, protein aggregation occurs in the ER, which evokes ER stress, leading to the activation of the unfolded protein response (UPR). The UPR system aims to restore normal cellular function and reduce ER stress. Failure to do so leads to major diseases, including neurodegenerative disorders, metabolic disorders, and cancer (27–29). Therefore, the ability to maintain a manageable level of ER stress is essential for human health.

Misfolded proteins can be targeted for degradation following the activation of the UPR system in multiple ways. A major way occurs through ER-associated degradation (ERAD), which involves the retro-translocation of misfolded proteins out of the ER followed by their ubiquitination for targeting to the proteasome. Another way involves transport out of the ER followed by targeting to the lysosome for degradation. It has also been demonstrated that mutations in GnRHR, identified in patients with HH, result in degradation that combines elements of both proteasomal and autophagic degradation (30).

With respect to the ERAD-based mechanism, it has been observed that some proteins are transported out of the ER and then retrieved from the Golgi back to the ER for degradation (31, 32). Why this occurs has been unclear. Here, we have studied in detail how a mutation at a residue in PROKR2, which is conserved across many GPCRs, affects its intracellular transport to alter function. Our results advance the understanding of disease pathogenesis induced by a key GPCR mutation and also contribute to a fundamental understanding of the different ways that misfolded proteins can be managed by the cell to maintain homeostasis.

Results

Trafficking-Defective PROKR2 Mutants Have Impaired Function Because of Loss of Cell Surface Expression. We initially studied PROKR2 mutants harboring L173R, W178S, or P290S missense mutations in transmembrane domain (TM) 4 or 6, which were previously identified in patients with HH or KS (Fig. 1A). W178 and P290 are the most highly conserved residues in TM4 and TM6 among GPCRs. It has been shown that these mutations reduce ligand-binding affinity, ligand-stimulated intracellular Ca^{2+} mobilization, and the cell surface expression of PROKR2. Furthermore, molecular modeling, based on the solved structures of rhodopsin and β 2-adrenergic receptor, predicts that these mutations would impair protein stability by impacting the correct folding of PROKR2 (17).

To further characterize cellular trafficking and function of WT PROKR2 and the three mutants, we constructed plasmids encoding PROKR2 with a 3xFLAG-3xHA (3F3H) tag at the C terminus or N terminus. The PROKR2 constructs tagged at the C terminus induced MAPK activity (as measured by induction of cotransfected Egr1-luciferase activity) in response to the PROKR2 ligand (prokineticin-2, or PK-2) in human embryonic kidney (HEK)293T cells, whereas constructs with N-terminal tags were unable to activate these downstream signaling pathways (*SI Appendix, Fig. S1A*). Therefore, for all subsequent experiments, except where indicated, we used WT and mutant PROKR2 with the 3F3H tag at the C terminus.

We initially analyzed the total protein expression of the different PROKR2 forms by immunoblotting (Fig. 1B, *Upper*). In cells transiently expressing WT PROKR2, we observed two bands smaller than 50 kilodalton (kDa) (indicated by solid black arrowheads) as well as a larger diffuse band of 55–70 kDa in size (indicated by an open arrowhead). In cells transiently expressing each of the three mutants, only the intermediate band was prominently observed, while the upper band was markedly reduced, and the lowest band was not seen. We hypothesized that the upper band represents the mature (fully

glycosylated) form of PROKR2 expressed on the cell surface, while the lack of this mature form for the PROKR2 mutants reflects their inability to reach the cell surface. As confirmation, we isolated cell surface proteins using a surface biotinylation assay. Biotinylated proteins were detected for the two upper bands of WT PROKR2, while no form of the PROKR2 mutants was detected by this assay (Fig. 1B, *Lower*).

Next, to gain insight into the intracellular distributions of the PROKR2 forms, WT or mutant forms were transiently expressed in COS-7 cells and then examined by confocal microscopy. As expected, WT PROKR2 was expressed on the plasma membrane and also had some intracellular distributions, including the ER, as reflected by some colocalization with an ER marker, calnexin (Fig. 1C). In contrast, L173R, W178S, and P290S PROKR2 had primarily intracellular distributions, including the ER, but no obvious distribution on the plasma membrane (Fig. 1C) (23). As confirmation, we also evaluated the glycosylation state of WT and mutant forms using Endo H, a deglycosylating enzyme that determines whether glycoproteins in the secretory pathway have passed through the medial Golgi. We found that only the upper “mature” band of WT PROKR2 was resistant to Endo H (Fig. 1D). Taken together, these results confirmed that a significant fraction of the WT PROKR2 can be transported to the plasma membrane, but the mutants are mostly retained internally.

To confirm that the mutant receptors are largely nonfunctional, we next assessed downstream signaling. PROKR2 is known to be a G_q -coupled receptor that activates the MAPK pathway and increases intracellular calcium following stimulation by its ligand PK-2. In the presence of PK-2, only cells transfected with WT PROKR2, but not L173R, W178S, or P290S PROKR2, showed a substantial increase in MAPK signaling as reflected by the induction of Egr1-luciferase activity (Fig. 1E). Similarly, WT PROKR2 induced a robust increase in fluorescence after treatment with PK-2 in a direct Fluo-4 calcium assay, which quantifies intracellular calcium levels (Fig. 1F). In contrast, the response was markedly reduced for L173R PROKR2 and completely ablated for W178S and P290S PROKR2, which had levels similar to those in control cells that expressed the empty (pcDNA) vector. In sum, WT PROKR2 is expressed on the cell surface and responds to ligand stimulation with the activation of G_q -coupled signaling pathways, whereas L173R, W178S, and P290S PROKR2 mutants do not have significant surface expression and are defective in downstream signaling.

Comparative Interactome Profiling of WT and P290S PROKR2. To gain insight into why the mutant forms of PROKR2 cannot reach the cell surface, we next pursued a comparative interactome study, which involves immunoprecipitation coupled to mass spectrometry (IP-MS). The P290 amino acid in PROKR2, located in TM6, is of particular interest, as it is highly conserved in many GPCRs, suggesting that this amino acid may have important roles in the proper folding and intracellular trafficking of PROKR2. Therefore, we chose the P290S mutant for comparison with WT PROKR2. A schematic outline of the IP-MS approach is shown in Fig. 2A. For these studies, we generated stable HEK293T cell lines expressing WT or P290S PROKR2 or expressing empty vector in control cells. We selected stable cell lines that expressed modest levels of PROKR2 forms to mimic their physiologic expression. Furthermore, we confirmed appropriate signaling responses by the different PROKR2 forms using the Fluo-4 calcium assay (*SI Appendix, Fig. S1B*).

We identified a total of 683 proteins that interacted with WT PROKR2, P290S PROKR2, or both. Of this total, 53 were present only in the WT PROKR2 interactome and thus considered to have selective interaction with WT PROKR2. On the other hand, 67 proteins were present only in the

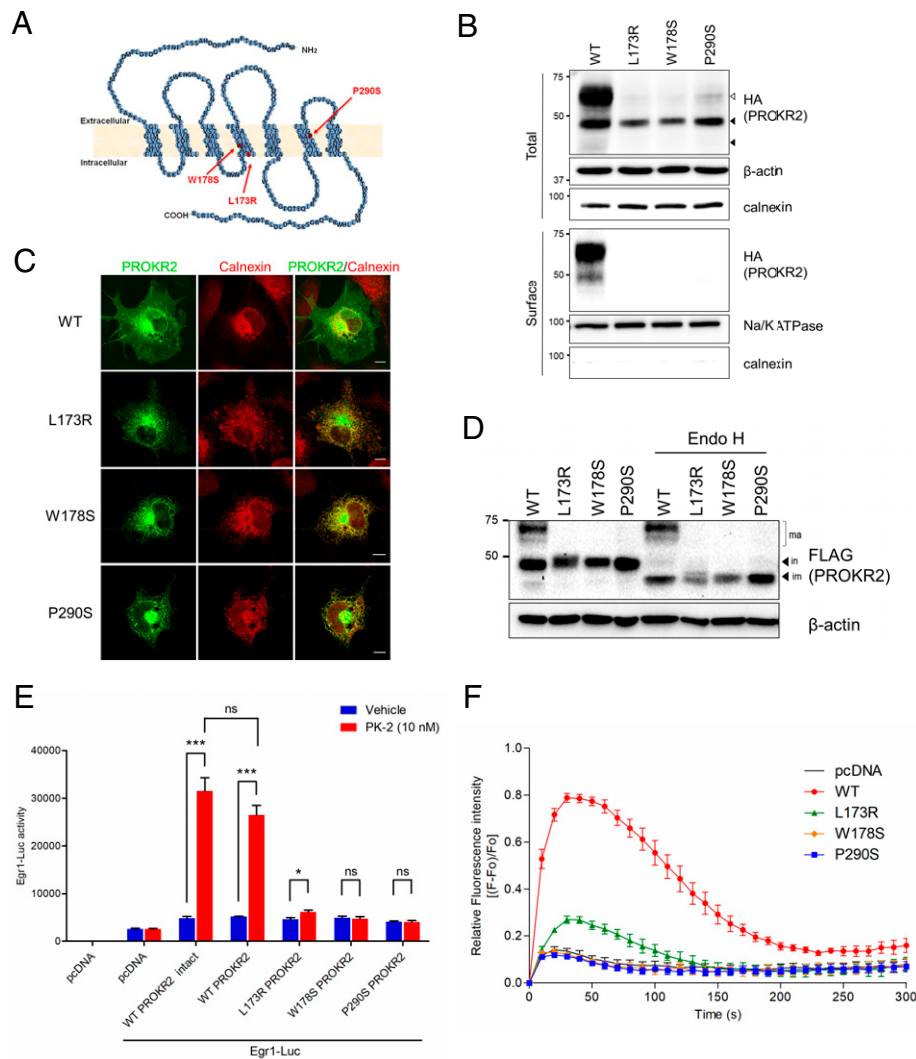


Fig. 1. Trafficking-defective mutants of PROKR2 lack cell surface expression and signaling activity. (A) Schematic representation of human PROKR2 with missense mutations L173R, W178S, and P290S indicated by red arrows. (B) Total and cell surface protein expression of WT, L173R, W178S, or P290S PROKR2. A cell surface biotinylation assay was performed in HEK293T cells expressing each PROKR2-3xHA construct. A fraction (10%) of the total cell lysate was immunoblotted (*Upper*), and biotinylated proteins were pulled down using streptavidin agarose and then immunoblotted (*Lower*). β -actin was used as a loading control. Calnexin and Na/K ATPase were used as markers for intracellular versus surface proteins, respectively. (C) Representative confocal images showing subcellular localization of WT, L173R, W178S, and P290S PROKR2. COS-7 cells expressing PROKR2-3F3H were coimmunostained with anti-HA (green) and anti-calnexin (red, an ER marker) antibodies. The third set of panels show colocalization of PROKR2 forms and calnexin. (Scale bars, 10 μ m.) (D) Glycosylation states of WT, L173R, W178S, and P290S PROKR2. The cell lysates expressing WT or mutant PROKR2-3F3H were treated with Endo H and then analyzed by immunoblotting with an anti-FLAG antibody. β -actin was used as a loading control; ma, mature; in, intermediate; im, immature bands are indicated. (E) Functional analysis of PROKR2 signaling using an Egr1-Luciferase (Egr1-Luc) reporter assay. A PROKR2-3F3H form (WT, L173R, W178S, or P290S) and Egr1-Luc were cotransfected in HEK293T cells. Intact WT PROKR2 (with no tag) was used to measure luciferase activity compared to WT PROKR2-3F3H. The cells were treated with vehicle or PK-2 (10 nM) 24 h after transfection for 16 h, after which cell lysates were harvested and luciferase activity measured. The bar graph shows mean \pm SEM of the luciferase activity from triplicate samples. *P* values were determined using paired one-tailed Student's *t* tests; **P* < 0.05; ****P* < 0.001; ns, not significant. (F) Functional analysis of PROKR2 signaling using an intracellular calcium assay. PROKR2-3F3H (WT, L173R, W178S, or P290S) or control (vector alone) were transiently transfected in COS-7 cells. The intracellular calcium mobilization in response to the addition of PK-2 (10 nM) was assessed 24 h after transfection by measuring fluorescence using the direct Fluo-4 calcium assay. Error bars represent mean \pm SEM of fluorescence intensity from triplicate experiments.

P290S PROKR2 interactome and thus considered to have selective interaction with P290S PROKR2. We further compared the proteins enriched in either the WT or P290S PROKR2 interactome. In this analysis, the proteins were filtered using a 1.5-fold enrichment cutoff. We found that 171 proteins were enriched in the WT PROKR2 interactome, while 215 proteins were enriched in the P290S PROKR2 interactome. These results are summarized in Fig. 2B, and all proteins identified in the interactome study are listed in *SI Appendix, Table S1*.

To compare predicted biological processes associated with either WT or P290S PROKR2-interacting proteins, we performed enrichment analysis by gene ontology (GO) using the Protein Analysis Through Evolutionary Relationships (PANTHER) database. The GO analysis for WT PROKR2 identified biological processes, including protein folding and membrane fusion, while P290S PROKR2 associated with pathways involved in ERAD, ER to Golgi transport, retrograde transport from Golgi to ER, and protein glycosylation (Fig. 2C). These notable biological processes associated with P290S PROKR2

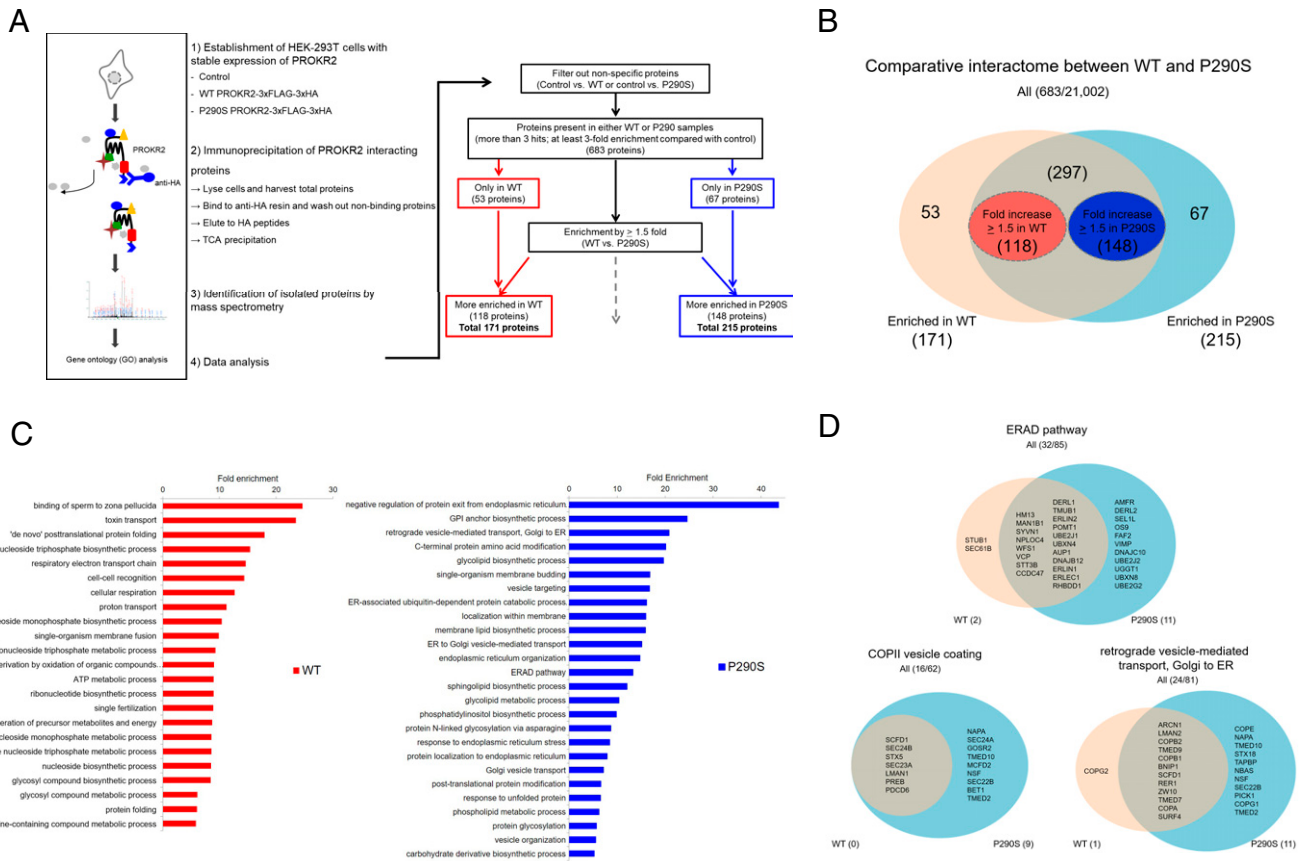


Fig. 2. Comparative interactome of WT versus P290S PROKR2. (A) Schematic overview of the IP-MS experimental design and decision tree for the identification of proteins interacting with WT versus P290S PROKR2-3F3H. (B) Venn diagrams of the numbers of proteins identified in the interactomes of WT or P290S PROKR2. The numbers of overlapping and unique interacting proteins are indicated. (C) GO analysis of proteins significantly enriched in either the WT (Left, red) or P290S (Right, blue) PROKR2 interactome using the PANTHER database. Enrichment for GO "Biological process" classifications of proteins detected in the interactomes of WT PROKR2 ($n = 171$; red bars) and P290S PROKR2 ($n = 215$; blue bars). (D) Venn diagrams of proteins enriched in the interactomes of WT or P290S PROKR2. The genes categorized into the selected biological processes are shown in the Venn diagrams.

are shown in Venn diagrams in which a comparison of proteins identified in the WT versus the P290S PROKR2 interactomes are further detailed (Fig. 2D).

WT and P290S PROKR2 Are Degraded by the ERAD Pathway. In the ER, protein-folding chaperones such as BiP bind to misfolded proteins to promote refolding. The impairment of this process results in misfolded proteins typically being targeted for ERAD. Thus, as a subset of identified interactors relate to ERAD, we initially sought confirmation that the mutant P290S PROKR2 undergoes ERAD by examining HEK293 cells that transiently express this mutant receptor. In the presence of cycloheximide (an inhibitor of protein synthesis), the immature forms of the receptor, which by endoH analysis (Fig. 1D) likely represent those that have not been transported out of the early secretory system, were observed to undergo degradation (Fig. 3A). Moreover, quantitation confirmed that the mutant receptor was degraded more rapidly than the WT receptor (Fig. 3A). It is worth further noting that this difference in the rate of degradation may be even greater than it appears since a portion of the decrease in the intermediate band for WT PROKR2 may be attributable to further processing to the mature form (upper band) rather than to degradation. In contrast, because P290S PROKR2 fails to undergo further maturation (as indicated by the absence of the upper band), all of the decline in its intermediate band is attributable to degradation.

To gain insight into the degradation mechanism involved, we next assessed protein stability in the presence of cycloheximide in

cells treated additionally with either MG132, a proteasome inhibitor, or chloroquine, an inhibitor of autophagic and lysosomal degradation. In the presence of MG132, both WT and P290S PROKR2 protein levels, when expressed transiently, were higher than in control cells, whereas chloroquine had no appreciable effect (Fig. 3B). We confirmed that L173R and W178S PROKR2 also showed sensitivity to MG132 but not to chloroquine (SI Appendix, Fig. S2A). We also confirmed that similar results were seen when the PROKR2 forms are expressed stably in cells, as WT and P290S PROKR2 displayed similar sensitivity to MG132 but not to chloroquine treatment (SI Appendix, Fig. S2B). As a technical note, we also wish to point out that the intensity of the upper (mature) band of WT PROKR2 varied depending on whether stable cell lines (which were selected to have a lower level of expression) or transiently transfected cells were studied. For the latter, the intensity of the upper band could further vary depending on the duration of the transient transfection.

To further confirm the findings in Fig. 3B, we also examined the behaviors of WT and P290S PROKR2 in the presence of bortezomib (another proteasome inhibitor), bafilomycin A1 (another autophagic and lysosome inhibitor), or wortmannin (blocker of autophagosome), which revealed that WT and P290S PROKR2 are sensitive to bortezomib (SI Appendix, Fig. S2C and D). Thus, these results further supported that both WT PROKR2 and the three trafficking-defective mutants are degraded through ERAD.

To further characterize this degradation, we next assessed if ubiquitination occurred. Both WT and P290S PROKR2

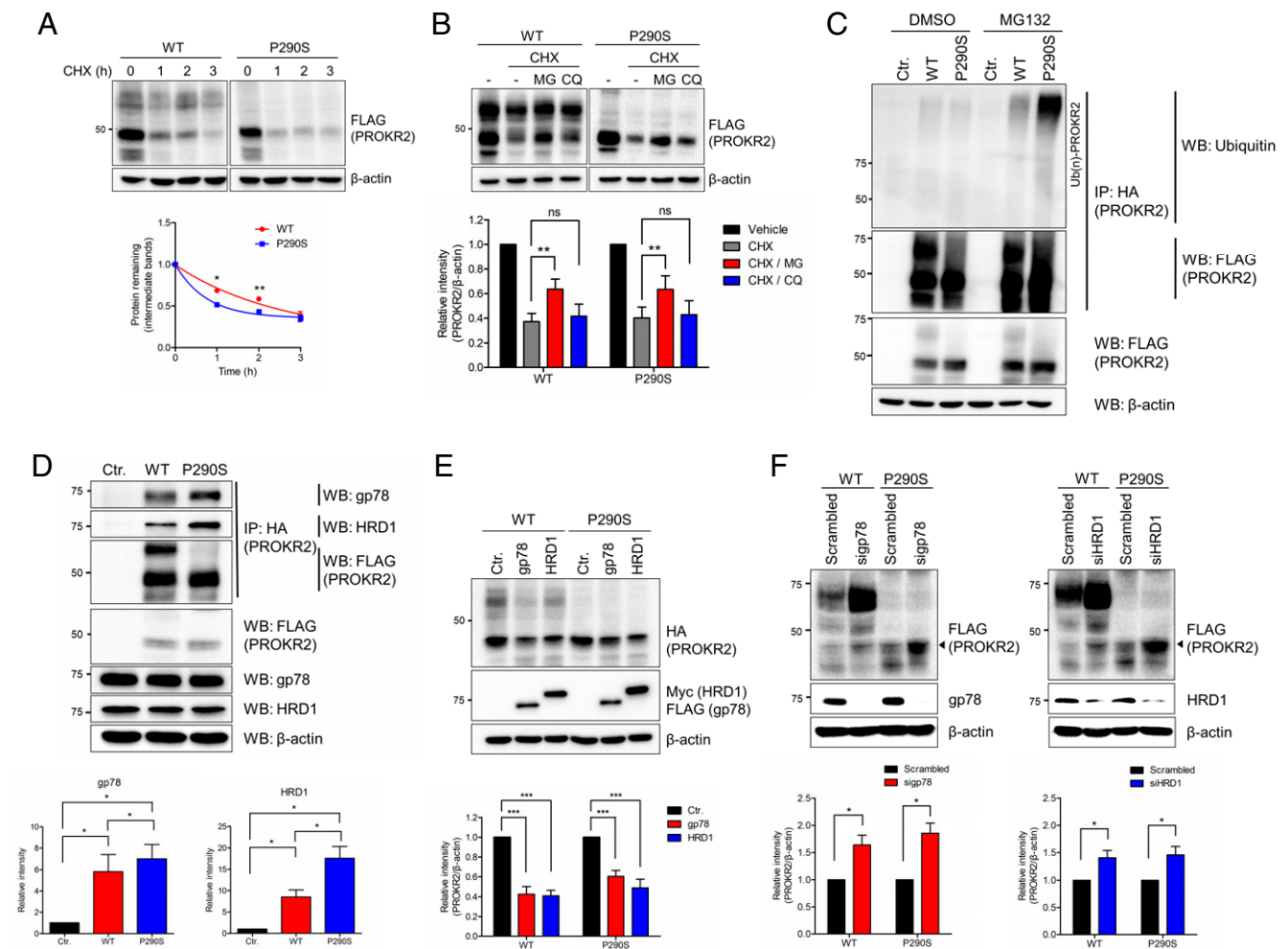


Fig. 3. WT and P290S PROKR2 are degraded via the ERAD pathway. (A) Stability of WT and P290S PROKR2 in transiently transfected HEK293T cells. The proteins were harvested 24 h after transfection in the presence of cycloheximide (CHX, 100 μ M) for the times indicated. (Upper) Representative immunoblot. (Lower) Quantification of protein remaining in the intermediate (Endo H sensitive) bands. β -actin was used as a loading control. The error bars represent mean \pm SEM of intermediate band intensity from three independent experiments. *P* values were determined using paired one-tailed Student's *t* tests; **P* < 0.05; ***P* < 0.01. (B) WT and P290S PROKR2 protein levels in transiently transfected HEK293T cells following treatment with the proteasome inhibitor MG132 (MG, 10 μ M) or the lysosome inhibitor chloroquine (CQ, 10 μ M) in the presence of CHX (100 μ M) for 3 h. (Upper) Representative immunoblot. (Lower) Quantification of the intermediate (Endo H sensitive) bands. The bar graph depicts mean \pm SEM of the intensity of the intermediate PROKR2 bands, normalized to β -actin, from four independent experiments. *P* values were determined using paired one-tailed Student's *t* tests; ***P* < 0.01; ns, not significant. (C) HEK293T cells with stable expression of WT or P290S PROKR2-3F3H or control cells expressing vector (pcDNA) were treated with MG132 or DMSO for 6 h followed by immunoprecipitation with an HA antibody and then were immunoblotted with an anti-ubiquitin antibody. A total of 10% of the total lysate was immunoblotted with the indicated antibodies (Lower), and 90% of total protein was used for immunoprecipitation followed by detection using the indicated antibodies (Upper). Ub(n)-PROKR2 indicates polyubiquitinated PROKR2 in Upper. (D) gp78 and HRD1 E3 ubiquitin ligases interact with both WT and P290S PROKR2. Immunoprecipitation was performed using an anti-HA antibody on cell lysates derived from HEK293T cells with stable expression of WT or P290S PROKR2-3F3H or control cells expressing pcDNA, and then gp78 and HRD1 were detected through immunoblotting. A total of 10% of total lysate was immunoblotted with the indicated antibodies (Lower), and 90% of total protein was used for immunoprecipitation followed by detection using the indicated antibodies (Upper). The relative intensities of the gp78 and HRD1 bands were normalized to the intensity in control cells that expressed pcDNA with quantitation shown in Lower. The bar graph values are mean \pm SEM from three independent experiments. *P* values were determined using paired one-tailed Student's *t* tests; **P* < 0.05. (E) HEK293T cells were cotransfected with gp78-FLAG, His/Myc-HRD1, or pcDNA (as control) and also with WT or P290S PROKR2-3xHA. PROKR2 protein levels were determined by immunoblotting (Upper). In Lower, quantitation of the intensity of the PROKR2 intermediate bands normalized to β -actin is shown; values are mean \pm SEM from five independent experiments. *P* values were determined using paired one-tailed Student's *t* tests; ****P* < 0.001. (F) Protein levels of WT or P290S PROKR2 were measured in transiently transfected HEK293T cells in the presence of siRNA that targets either gp78 (Left) or HRD1 (Right). Scrambled siRNA was used as a control. The bar graph values are mean \pm SEM of the intermediate bands (indicated by solid black arrowheads) from three independent experiments. *P* values were determined using paired one-tailed Student's *t* tests; **P* < 0.05.

underwent ubiquitination, which was more apparent in the presence of MG132, with P290S PROKR2 being ubiquitinated to a greater extent (Fig. 3C). We next considered that the interactome results had suggested that gp78 (also known as AMFR) associates more strongly with P290S than with WT PROKR2, whereas HRD1 (also known as SYVN1) interacts similarly with

WT and P290S PROKR2. As these E3 ligases are known to act in ERAD, we investigated their roles in PROKR2 degradation. The results revealed that both WT and P290S PROKR2 interact with gp78 and HRD1 proteins, with stronger interactions occurring for P290S than for WT PROKR2 (Fig. 3D). To confirm that WT and P290S PROKR2 are substrates of both gp78

and HRD1 in the ERAD pathway, we next investigated the effect of altering the expression level of these E3 ligases. When gp78 was overexpressed, both WT and P290S PROKR2 levels were decreased (Fig. 3E). Similar effects were observed with the overexpression of HRD1 (Fig. 3E). We also examined the effects of reducing the levels of either gp78 or HRD1. When gp78 expression was reduced by small interfering RNA (siRNA), protein levels of both WT and P290S PROKR2 were increased (Fig. 3F). Similarly, the knockdown of HRD1 led to the accumulation of both WT and P290S PROKR2 (Fig. 3F). Collectively, the results further supported that WT and P290S PROKR2 are degraded via the ERAD pathway rather than the lysosomal pathway, with P290S PROKR2 being more susceptible to ERAD than WT PROKR2.

Both WT and P290S PROKR2 Are Transported to the Golgi. We next noted that the interactome analysis identified proteins involved in transport between the ER and the Golgi. Guided by this observation, we performed confocal microscopy and found that both WT and P290S have a significant distribution at the Golgi (Fig. 4A). The L173R and W178S PROKR2 mutants also exhibited a significant distribution at the Golgi (SI Appendix, Fig. S3A). The finding that WT PROKR2 exits the ER was expected, as a significant fraction of the WT had been detected at the plasma membrane. However, the finding that the P290S mutant also exits the ER was surprising, as it would have been expected to be retained in the ER for disposal by ERAD. Thus, to further confirm that the P290S mutant exits the ER, we found that, like the WT, the mutant also associates with Sec24B (Fig. 4B), a component of the coat protein complex II (COPII) machinery that forms transport carriers for exit from the ER. This result was also confirmed by examining the degree to which Sec24B associates with the WT and P290S receptor (SI Appendix, Fig. S3B). As such, we next sought insight into why the mutant PROKR2 exits the ER.

Transport of P290S PROKR2 to the Golgi Relieves ER Stress. A previous study had shown that the exit of misfolded GPI-anchored proteins from the ER provides a way to reduce ER stress by preventing the oversaturation of the ER folding capacity (33). In this case, the exit from the ER leads to misfolded proteins being targeted to the lysosomal pathway for degradation. As such, we hypothesized that the exit of the mutant (P290S) PROKR2 from the ER also reduces ER stress. However, because the P290S PROKR2 is disposed by ERAD, a different post-ER itinerary would be predicted for this mutant PROKR2. Thus, we next pursued studies to test these predictions.

We initially sought to detect ER stress by measuring the messenger RNA (mRNA) levels of BiP, CHOP, and spliced XBP1 (sXBP1) through qRT-PCR. However, we could not detect an appreciable increase in these levels when comparing cells that expressed P290S PROKR2 to those that expressed WT PROKR2 or to control cells (Fig. 4C). As a positive control, we found that cells treated with dithiothreitol (DTT) for 1 h showed increased level of CHOP and sXBP1 mRNA levels (Fig. 4C), while a longer exposure to DTT (6 h) resulted in BiP mRNA levels also becoming elevated (SI Appendix, Fig. S3C).

We next considered that the expression of a single mutant protein in the context of the myriad of proteins that exist in the ER may not induce sufficient ER stress to be detected by conventional means. Thus, we sought more sensitive approaches. As one approach, we found that BiP exhibits a greater association with the P290S mutant compared to that of WT PROKR2 (Fig. 4D). As another approach, we were led by the consideration that ER stress can be alleviated by multiple response pathways. Thus, we reasoned that crippling one pathway may result in the ER being more sensitive to stress. Aldehyde 8-formyl-7-hydroxy-4-methylcoumarin (4u8C) has been shown to

inhibit one ER stress response pathway mediated by IRE1 (34–37). When cells were treated with 4u8C for 1 h, we found that BiP and CHOP mRNA levels were induced by 1.4- and twofold, respectively, as compared to untreated cells (see control conditions in Fig. 4E). As a positive control, DTT treatment further increased these levels (Fig. 4E). In contrast, DTT treatment did not increase sXBP1 mRNA levels (Fig. 4E), which was expected because this readout measures the IRE1 pathway, which is incapacitated by 4u8C treatment. As another control, we examined the effect of treating cells with brefeldin-A (BFA). This pharmacologic agent prevents the ER exit, which is predicted to induce ER stress. We found that BFA treatment by itself induced a marginal level of ER stress, which becomes more pronounced when 4u8C was added (SI Appendix, Fig. S3D). We then found that cells expressing WT PROKR2 had similar levels of CHOP mRNA as compared to control cells in the presence of the 4u8C. However, the cells expressing P290S PROKR2 showed a further increase in the CHOP mRNA levels (Fig. 4E). Thus, through 4u8C treatment, we achieved a more sensitive way of detecting ER stress induced by the expression of P290S PROKR2.

We next sought to determine whether the transport of the P290S mutant out of the ER reduces ER stress. Appending the KKxx motif to the C terminus of transmembrane proteins has been shown to enhance their ER localization (38). We first confirmed that appending the KKxx motif also results in the mutant P290S PROKR2 having a greater distribution in the ER (Fig. 4F). Consistent with this finding, immunoblotting revealed that appending the KKxx motif to the C terminus of the WT PROKR2 eliminates its higher molecular mass (mature) form (SI Appendix, Fig. S3E). Notably, we then found that appending the KKxx motif to the mutant P290S PROKR2 results in enhanced ER stress in cells treated with 4u8C as assessed through CHOP mRNA levels (Fig. 4G). Thus, these results revealed that the exit of the mutant P290S PROKR2 from the ER provides a way of reducing ER stress.

P290S PROKR2 Is Retrieved from Golgi to ER for Disposal by ERAD. In considering how the exit from the ER could still lead to the mutant P290S PROKR2 being disposed by ERAD, we were next guided by the interactome results that had found this mutant to associate with components of the COPI complex, which is known to mediate retrograde transport from the Golgi to the ER (39). Thus, we next examined the effect of blocking COPI transport on the intracellular distribution of the mutant P290S PROKR2.

As a technical consideration, we noted that targeting subunits of coatomer, which form the core components of the COPI complex, not only inhibits COPI cargo transport but also disrupts the Golgi complex (40). To overcome this conundrum, we noted that ARFGAP1 is another component of the COPI complex, and targeting against this auxiliary component has been shown to inhibit COPI cargo transport while leaving the Golgi intact (41). Using siRNA to reduce ARFGAP1 expression, we found that the protein level of mutant P290S PROKR2 increased compared to that of WT PROKR2 (Fig. 5A). We also performed kinetic analysis by treating cells with cycloheximide and then comparing the stability of WT versus mutant, which confirmed that siRNA against ARFGAP1 has a selective effect on the protein stability of the mutant PROKR2 (Fig. 5B and C).

We also found that ARFGAP1 knockdown results in the mutant P290S PROKR2 having a greater distribution at the Golgi (Fig. 5D). Moreover, we found that the mutant P290S PROKR2 shows greater association with β -COP (Fig. 5E), a component of the COPI complex (42). Thus, these results suggested that the mutant P290S PROKR2, upon reaching the Golgi, is retrieved to the ER through the COPI pathway.

We also examined the possibility that the inhibition of this retrograde transport could result in mutant P290S PROKR2

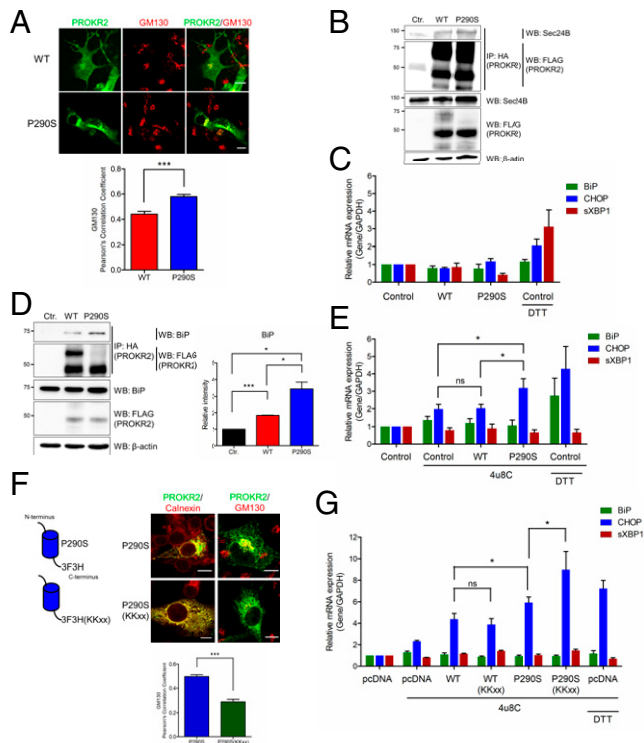


Fig. 4. P290S PROKR2 is transported out of the ER to reduce ER stress. (A) Colocalization of WT and P290S PROKR2 with GM130, a *cis*-Golgi marker, in COS-7 cells. WT or P290S PROKR2–3F3H were transiently transfected into COS-7 cells, and then cells were immunostained with anti-HA (green) and anti-GM130 (red) antibodies. Images were acquired using a Leica SPE confocal microscope (Upper), and colocalization was quantified using ImageJ software. (Scale bars, 10 μ m.) The bar graph (Lower) represents Pearson's correlation coefficient of WT or P290S PROKR2 with GM130, and values are mean \pm SEM from 50 to 100 cells in 10 to 20 fields. *P* values were determined using unpaired one-tailed Student's *t* tests; ****P* < 0.001. (B) Sec24B interacts with WT and P290S PROKR2. HEK293T cells with a stable expression of WT or P290S PROKR2–3F3H were used to assess their interaction with Sec24B. A total of 10% of total lysate was immunoblotted with indicated antibodies (Lower), and 90% of total protein was used for immunoprecipitation by HA antibody followed by detection using the indicated antibodies (Upper). (C) Relative mRNA levels of BiP, CHOP, and sXBP1 in cells expressing WT or P290S PROKR2. BiP, CHOP, and sXBP1 mRNA levels were measured in HEK293T cells with stable expression of WT or P290S PROKR2–3F3H or pcDNA as a negative control. In addition, control cells expressing pcDNA were treated with DTT (1 mM; 1 h) as a positive control for detection of ER stress. mRNA levels were normalized to that of GAPDH for quantitation. The bar graph values are mean \pm SEM of relative mRNA expression from three independent experiments. (D) BiP protein associates with WT and P290S PROKR2. Immunoprecipitation was performed on HEK293T cells with stable expression of WT or P290S PROKR2 or control cells expressing pcDNA using an anti-HA antibody followed by immunoblotting for proteins as indicated. A total of 10% of total lysate was used for immunoblotting, and 90% of total protein was used for immunoprecipitation. A representative experiment is shown on Left, while quantitation from three independent experiments is shown on Right. Bars represent mean \pm SEM with *P* values determined using paired one-tailed Student's *t* tests. **P* < 0.01. ****P* < 0.001. (E) Relative mRNA levels of BiP, CHOP, and sXBP1 with or without 4u8C treatment (500 μ M; 1 h) in HEK293T cells with stable expression of WT or P290S PROKR2 or pcDNA as a negative control. DTT (1 mM; 1 h) was added in addition to 4u8C to cells expressing pcDNA as a positive control. Bars represent mean \pm SEM of relative mRNA expression from three independent experiments. *P* values were determined using paired one-tailed Student's *t* tests. **P* < 0.05. ns, not significant. (F) Relative distributions of P290S and P290S(KKxx) PROKR2 in the ER and Golgi. The KKxx motif was appended to the C terminus of P290S PROKR2–3F3H (Left). Intracellular distribution of P290S and P290S(KKxx) PROKR2 was assessed by immunostaining (Right Upper). P290S and P290S(KKxx) PROKR2 were transfected into COS-7 cells and

being rerouted from the Golgi to either the lysosomal pathway for degradation or to the plasma membrane. However, when cells were treated with chloroquine, we found that siRNA against ARFGAP1 did not induce an increased level of the mutant P290S PROKR2 (SI Appendix, Fig. S4A), which ruled against the diversion from the Golgi to the lysosome for degradation. Moreover, siRNA against ARFGAP1 did not enhance the cell surface detection of the mutant P290S PROKR2 (SI Appendix, Fig. S4B), which ruled against the diversion from the Golgi to the plasma membrane.

RER1 Links P290S PROKR2 to the COPI Pathway. We next considered that the COPI complex recognizes dilysine-based motifs at the C terminus of transmembrane cargo proteins for their retrograde transport from the Golgi to the ER (43). However, PROKR2 does not possess this motif at its C terminus. Thus, how can PROKR2 be transported through the COPI pathway? As an alternative to direct binding by the COPI complex, cargo proteins can also engage the COPI complex indirectly through transmembrane proteins known as cargo receptors. Such a situation would also explain why we had observed a relatively weak interaction between the mutant P290S PROKR2 and β -COP (Fig. 5E). Thus, we next examined whether a cargo receptor links mutant P290S PROKR2 to the COPI complex.

A particularly well-known cargo receptor of the COPI pathway is the Lys-Asp-Glu-Leu (KDEL) receptor, which binds soluble luminal proteins that possess the KDEL motif at their C terminus and retrieves them from the Golgi to the ER (39). Many protein-folding chaperones in the ER possess the KDEL motif, including BiP, and are known to be transported to the Golgi and then retrieved to the ER through the KDEL receptor (44). Thus, as we had detected an interaction between the mutant P290S PROKR2 and BiP (Fig. 4D), one possibility could be that the mutant P290S PROKR2 is transported through the COPI pathway by interacting with KDEL-bearing chaperones that can engage the KDEL receptor (Fig. 6A, model *i*). Alternatively, RER1 has been shown to bind transmembrane cargo proteins and link them to the COPI complex for retrograde transport from the Golgi to the ER (45–48). Thus, another possibility could be that the mutant P290S PROKR2 is transported through the COPI pathway through association with RER1 (Fig. 6A, model *ii*). Performing coprecipitation experiments, we found that neither P290S nor WT PROKR2 shows an appreciable association with the KDEL receptor (Fig. 6B), while both forms have an appreciable association with RER1, with the mutant PROKR2 associating with RER1 better than the WT PROKR2 (Fig. 6B). It is further notable that these results are consistent with our interactome results which had revealed PROKR2 to associate with RER1 but not with the KDEL receptor (Fig. 2D).

We then pursued functional studies to further confirm that RER1, but not the KDEL receptor, acts to retrieve the mutant P290S PROKR2 from the Golgi to the ER. Performing siRNA studies, we found that targeting RER1, but not the KDEL

then immunostained using anti-HA (green) and either anti-calnexin or anti-GM130 (red) antibodies (Right). (Scale bars, 10 μ m.) The graph (Right Lower) depicts Pearson's correlation coefficient between PROKR2 receptors and GM130. Bars represent mean \pm SEM. *P* values were determined using unpaired one-tailed Student's *t* tests; ****P* < 0.001. (G) Relative mRNA levels of BiP, CHOP, and sXBP1 in HEK293T cells transiently transfected with WT, WT(KKxx), P290S or P290S(KKxx) PROKR2, or pcDNA (as vector control). Total RNA was harvested 24 h after transfection from cells treated with or without 4u8C. The cells transfected with pcDNA were treated with 4u8C with or without DTT for control comparisons. Bars represent mean \pm SEM of relative mRNA levels from four independent experiments. *P* values were determined using paired one-tailed Student's *t* tests. **P* < 0.05. ns, not significant.

receptor, results in the mutant P290S PROKR2 having increased localization at the Golgi (Fig. 6C). Moreover, this effect of siRNA against RER1 was reversed by rescue using an siRNA-

resistant form of RER1 (Fig. 6D). We also confirmed that siRNA against RER1 results in less mutant receptor localizing at the ER (Fig. 6E). Consistent with these results, we also found that

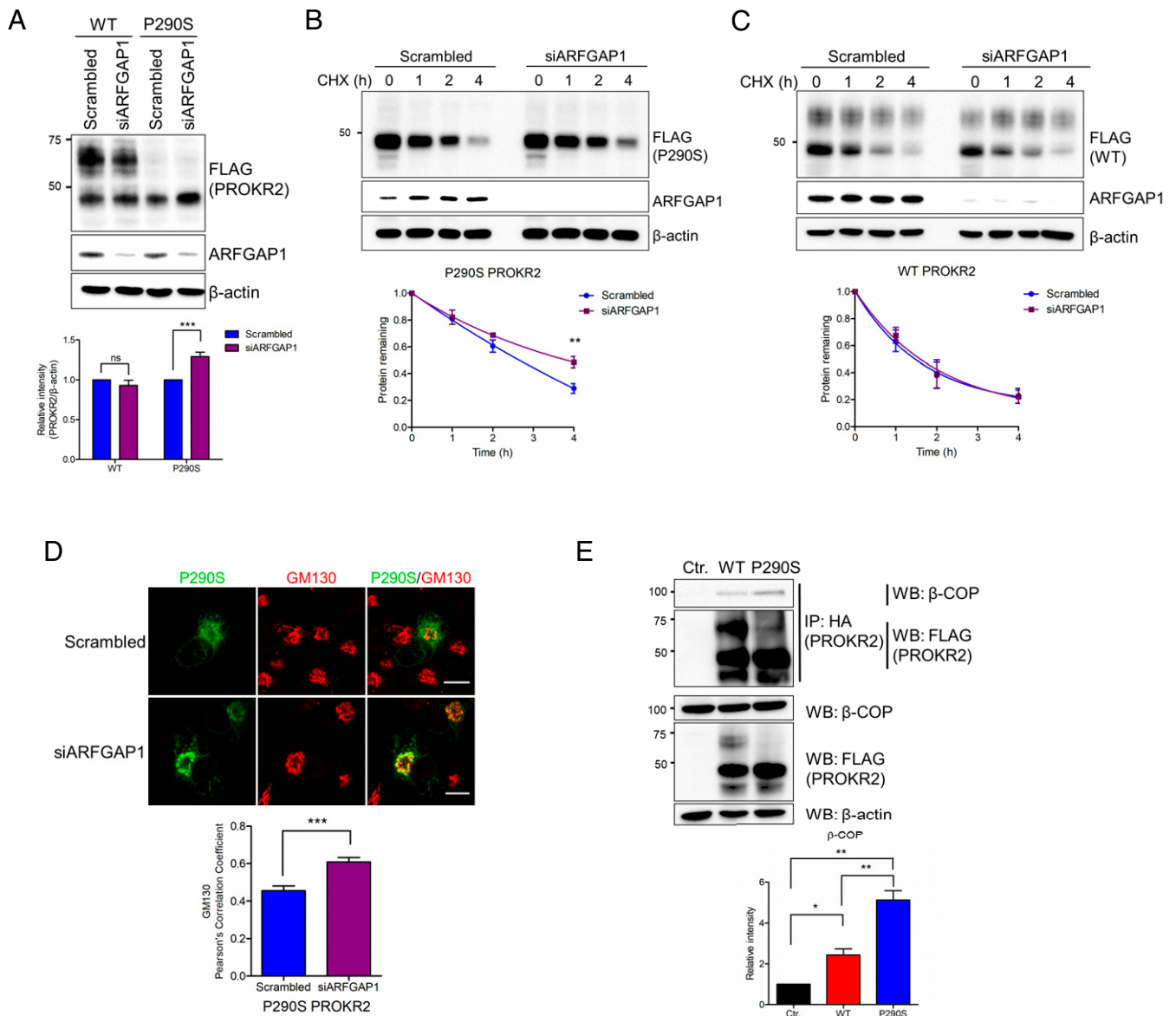


Fig. 5. P290S PROKR2 undergoes retrieval from the Golgi to the ER for degradation. (A) Protein levels of WT and P290S PROKR2 from transiently transfected HEK293T cells in the presence of siRNA against ARFGAP1 or scrambled siRNA were compared by immunoblotting (Upper). Quantitation (Lower) depicts the mean \pm SEM of the intensity of the intermediate PROKR2 band, normalized to β -actin, from eight independent experiments. *P* values were determined using paired one-tailed Student's *t* tests; ****P* < 0.001; ns, not significant. (B) Rate of degradation of P290S PROKR2 in HEK293T cells transfected with siRNA against ARFGAP1 or scrambled siRNA. Cycloheximide (CHX; 100 μ g/mL) was added to the cells 72 h after siRNA transfection, and the rate of P290S PROKR2 protein degradation was quantified. Upper shows representative immunoblot, while Lower shows quantitation of the rate of P290S protein degradation as reflected by intensity of the intermediate bands; values represent mean \pm SEM from three independent experiments. *P* values were determined using paired one-tailed Student's *t* tests; ***P* < 0.01. (C) Rate of degradation of WT PROKR2 in HEK293T cells transfected with siRNA against ARFGAP1 or scrambled siRNA. CHX (100 μ g/mL) was added to the cells 72 h after siRNA, and the rate of WT PROKR2 protein degradation was measured. Upper shows representative immunoblot, while Lower shows quantitation of the rate of WT PROKR2 protein degradation as reflected by relative intensity of the intermediate bands; values represent mean \pm SEM from three independent experiments. (D) Colocalization of P290S PROKR2 with the Golgi marker GM130 as assessed by confocal microscopy. COS-7 cells were cotransfected with P290S PROKR2 and siRNA against ARFGAP1 or scrambled siRNA. P290S PROKR2 and GM130 were immunostained using anti-HA (green) and anti-GM130 (red) antibodies, respectively (Upper). (Scale bars, 10 μ m.) Quantitation (Lower) shows Pearson's correlation coefficient between P290S PROKR2 and GM130. The bar graph shows mean \pm SEM from quantitation of 50 to 100 cells in 10 to 20 fields. *P* values were determined using unpaired one-tailed Student's *t* tests; ****P* < 0.001. (E) COPI interacts with WT and P290S PROKR2. HEK293T cells with stable expression of WT or P290S PROKR2 or pcDNA as a negative control were immunoprecipitated for PROKR2 followed by immunoblotting for β -COP, a component of the COPI complex. A total of 10% of total lysate was immunoblotted with the indicated antibodies (lower section in Upper), and 90% of total protein was used for immunoprecipitation followed by detection using the indicated antibodies (upper section in Upper panel). Relative intensity of immunoprecipitated β -COP was determined using ImageJ (Lower). Quantitation shows mean \pm SEM of immunoprecipitated β -COP from three independent experiments. *P* values were determined using paired one-tailed Student's *t* tests; **P* < 0.05; ****P* < 0.01.

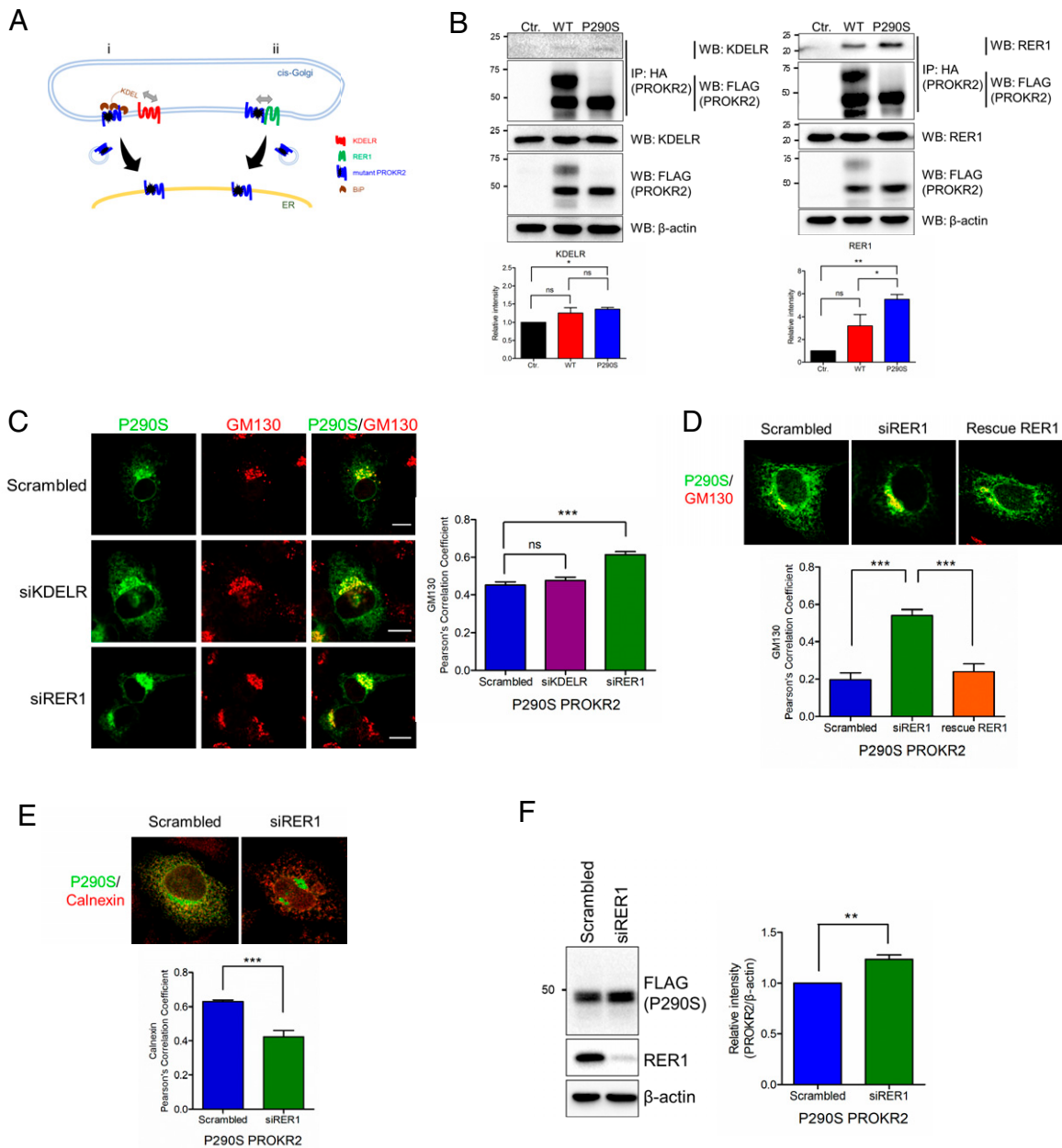


Fig. 6. RER1 is involved in retrograde transport of P290S PROKR2. (A) Schematic model of the retrieval of P290S PROKR2 from the Golgi to the ER through a cargo receptor. The KDEL receptor can link P290S PROKR2 to the COPI complex through its ligands, which are KDEL-bearing ER chaperones that can interact with P290S PROKR2 1), or RER1 can also link P290S PROKR2 to the COPI complex 2). (B) Assessing interactions between cargo receptors (KDEL or RER1) and WT or P290S PROKR2. Immunoprecipitation was performed using an anti-HA antibody directed against PROKR2-3F3H (WT or P290S) that were stably expressed in HEK293T cells. Control cells were stably expressed vector (pcDNA). A total of 10% of total lysate was immunoblotted with the indicated antibodies (lower section in *Upper*), while 90% of the total lysate was used for immunoprecipitation followed by detection using the indicated antibodies (upper section in *Upper*). Quantitation shows mean \pm SEM of intensity of immunoprecipitated KDEL or RER1, respectively, from three independent experiments (*Lower*). *P* values were determined using paired one-tailed Student's *t* tests; **P* < 0.05; ***P* < 0.01; ns, not significant. (C) The Golgi distribution of P290S PROKR2 is enhanced by siRNA against RER1 but not by siRNA against the KDEL receptor. P290S PROKR2-3F3H and GM130, a Golgi marker, were immunostained using anti-HA (green) and anti-GM130 (red) antibodies, respectively. (Scale bars, 10 μ m.) Quantitation shows Pearson's correlation coefficient between P290S and GM130. Values are shown as mean \pm SEM. *P* values were determined using unpaired one-tailed Student's *t* tests; ****P* < 0.001; ns, not significant. (D) The enhanced Golgi distribution of P290S PROKR2 induced by siRNA against RER1 is reversed upon rescue of RER1. HeLa cells were cotransfected with P290S PROKR2 and siRNA against RER1 or additionally with siRNA-resistant RER1. P290S PROKR2 and GM130 were immunostained using anti-HA (green) and anti-GM130 (red) antibodies, respectively (*Upper*). Colocalization of P290S PROKR2 with GM130 was quantified (*Lower*). Values are shown as mean \pm SEM. *P* values were determined using unpaired one-tailed Student's *t* tests; ****P* < 0.001. (E) The level of P290S PROKR2 in the ER is reduced by siRNA against RER1. HeLa cells were cotransfected with P290S PROKR2 and siRNA against RER1 or scrambled siRNA. P290S PROKR2 and calnexin were immunostained using anti-HA (green) and anti-calnexin (red) antibodies, respectively (*Upper*). Colocalization of P290S PROKR2 with calnexin was quantified (*Lower*). Values are shown as mean \pm SEM. *P* values were determined using unpaired one-tailed Student's *t* tests; ****P* < 0.001. (F) Silencing RER1 prevents the degradation of P290S PROKR2. Protein level was quantified in the P290S PROKR2-3F3H-expressing stable cells transfected with either siRNA against RER1 or scrambled siRNA. Immunoblot is shown on *Left*, and quantitation is shown on *Right*. Values reflect the mean \pm SEM of the intensity of the intermediate bands of P290S PROKR2 from four independent experiments. *P* values were determined using paired one-tailed Student's *t* tests; ***P* < 0.01.

siRNA against RER1 increased the protein level of the mutant P290S PROKR2 in cells (Fig. 6F).

The Key Findings for P290S PROKR2 Are Applicable to Another Model GPCR. We next examined whether these findings for PROKR2 could have broader implications, as the P290S mutation involves a proline that resides in TM6 of PROKR2, which is conserved among many GPCRs. Examining a model GPCR known as muscarinic acetylcholine receptor M3 (CHRM3), we found that mutating the conserved proline in this GPCR (P506S) also reduces its stability in cells (Fig. 7A). Moreover, in contrast to the WT form, the mutant P506S CHRM3 does not acquire a higher molecular mass form (Fig. 7A), suggesting that the mutant cannot reach the cell surface. As confirmation, we performed confocal microscopy and found that, in contrast to the WT form, the P506S mutant does not exhibit a significant distribution at the plasma membrane (Fig. 7B). Moreover, similar to P290S PROKR2, the P506S CHRM3 shows a significant distribution at the Golgi (Fig. 7B).

We next found that siRNA against ARFGAP1 increases the protein level of the mutant P506S CHRM3 in cells (Fig. 7C). Moreover, this siRNA treatment increased the localization of the P506S CHRM3 at the Golgi (Fig. 7D). Finally, examining ER stress by treating cells with 4u8C as we had done in studying PROKR2, we found that enhancing the ER localization of the mutant P506S CHRM3, by appending the KKxx motif to its C terminus, results in enhanced ER stress (Fig. 7E).

Discussion

Newly synthesized proteins in the ER are subjected to quality control surveillance in determining whether they can exit this compartment (49, 50). The proteins that do not pass this check are typically retained in the ER for disposal through ERAD. In this study, we have uncovered an exception to this generalization, finding a key role for post-ER transport to the Golgi in determining whether proteins are transported to the cell surface or returned to the ER for disposal by ERAD. We have also elucidated two major reasons for this post-ER itinerary. First, it enables the cell to distinguish WT from mutant proteins when the traditional ER-based mechanism falls short in this role. Second, the post-ER itinerary reduces ER stress by keeping the level of a misfolded protein to a manageable level in the ER.

We initially pursued a comparative interactome analysis, which revealed that a mutant (P290S) PROKR2, identified in patients with HH and KS and shown to have impaired function because of the loss of cell surface expression, is associated with proteins involved in biological processes that include protein folding and ERAD. Interestingly, the mutant PROKR2 is also associated with proteins related to the transport between the ER and the Golgi, including components of COPI and COPII complexes. These findings guided us to reveal that the mutant PROKR2 cycles between the ER and Golgi through the sequential engagement of the COPII machinery for the exit from the ER and then the COPI machinery for retrieval from the Golgi to the ER. In the latter case, we further elucidated that the transport of the mutant P290S PROKR2 in the COPI pathway involves its interaction with RER1, which acts as a cargo receptor in linking the mutant PROKR2 to the COPI machinery. Notably, we then discovered that this post-ER itinerary of the mutant PROKR2 helps to reduce ER stress by reducing its level in the ER while still allowing its ultimate disposal through ERAD.

Other proteins have been found previously to also exit the ER and then be retrieved from the Golgi to the ER for disposal by ERAD (32, 51–53). However, it has been unclear why this occurs. Our explanation that this post-ER itinerary provides a way to reduce ER stress was initially suggested by the observation that a higher level of BiP is found to associate with the

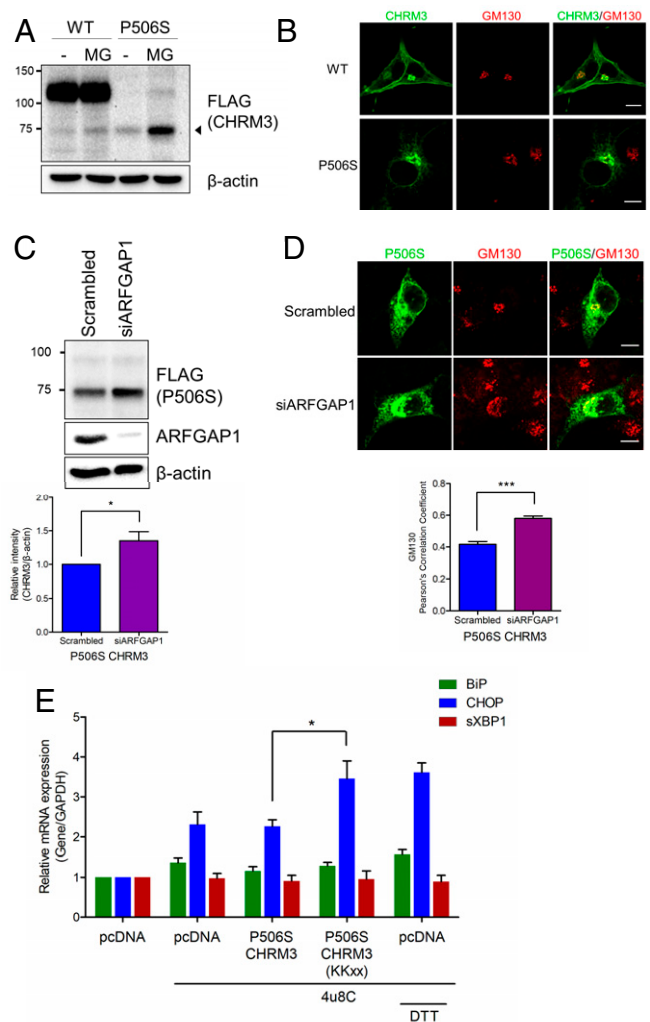


Fig. 7. Cycling between ER and Golgi also reduces ER stress for another model GPCR. (A) HEK293T cells expressing WT or P506S CHRM3–3F3H with or without MG132 (MG; 10 μ M; 6 h) were examined by immunoblotting using antibodies as indicated. β -actin was used as a loading control. (B) COS-7 cells transiently expressing WT or P506S CHRM3–3F3H were immunostained with anti-HA (green) and anti-GM130 (red) antibodies followed by imaging with confocal microscopy. (Scale bars, 10 μ m.) (C) P506S CHRM3 protein levels were assessed by immunoblotting of lysates derived from HEK293T cells that were transiently transfected with P506S CHRM3 and also treated with siRNA against ARFGAP1 or scrambled siRNA (Upper). Quantitation (Lower) shows mean \pm SEM intensity of the immature bands from five independent experiments. *P* values were determined using paired one-tailed Student's *t* tests; **P* < 0.05. (D) Colocalization of P506S CHRM3 with GM130 as assessed by confocal microscopy. COS-7 cells expressing P506S CHRM3–3F3H were transfected with siARFGAP1 or scrambled siRNA. P506S CHRM3 and GM130 were then immunostained using anti-HA (green) and anti-GM130 (red) antibodies, respectively. (Scale bars, 10 μ m.) Quantitation shows Pearson's correlation coefficient between P506S CHRM3 and GM130. Values reflect mean \pm SEM from 50 to 100 cells in 10 to 20 fields (Lower). *P* values were determined using unpaired one-tailed Student's *t* tests; ****P* < 0.001. (E) The relative mRNA levels of BiP, CHOP, and sXBP1 in HEK293T cells transiently expressing WT or P506S CHRM3. Total RNA was harvested 24 h after transfection from cells treated without or with 4u8C. The cells transfected with pcDNA were treated with 4u8C with or without DTT as controls. Quantitation shows mean \pm SEM of relative mRNA levels from six independent experiments. *P* values were determined using paired one-tailed Student's *t* tests; **P* < 0.05.

mutant P290S PROKR2 as compared to the WT counterpart. We confirmed this explanation through a more sensitive way of detecting ER stress by blocking one arm of the ER stress

response (mediated by the IRE1 pathway), which then allowed us to show that enhancing the ER localization of the mutant PROKR2 (by appending a KKxx motif to the C terminus) results in increased ER stress.

We have also uncovered another key reason for why the mutant P290S PROKR2 undergoes this more complex itinerary for ultimate disposal by ERAD. In contrast to the usual circumstance, when the ER-based quality control system can efficiently distinguish properly folded versus misfolded proteins in determining whether a protein becomes targeted to ERAD, we have found that this is not the case for the PROKR2, as both the WT and the P290S mutant are susceptible to ERAD. However, by having both proteins transported out of the ER and then having their ultimate fate being determined at the level of the Golgi with the WT allowed to transit further to the cell surface while the mutant is retrieved from the Golgi to the ER, the post-ER itinerary acts essentially as an additional quality control system when the traditional ER-based mechanism fails to function efficiently in distinguishing WT versus mutant protein.

We have also pursued further studies to suggest that our findings have broader applicability beyond PROKR2. The proline residue in TM6 of PROKR2 (P290) is highly conserved among GPCRs. Examining CHRM3 as another model GPCR, we find that mutating this conserved proline in TM6 of CHRM3 to serine (P506S) also results in a significant fraction of CHRM3 becoming distributed to the Golgi. Moreover, further analysis suggests that the mutant P506S CHRM3 similarly undergoes cycling between the ER and the Golgi as a way to reduce ER stress while also being disposed by ERAD.

Trafficking-defective mutant receptors have had cell surface transport restored by chemical chaperones such as glycerol or dimethyl sulfoxide (DMSO) as well as by pharmacological chaperones, which are selective antagonists or agonists to the receptors. As previously shown, glycerol, thought to broadly promote protein folding by decreasing the solvent-accessible surface area of the protein, promoted the cell surface transport of both W178S and P290S PROKR2 (23). In addition, A457, a pharmacological chaperone of PROKR2, was shown to functionally rescue P290S, but not W178S, PROKR2 (23). It was speculated that the inability of A457 to rescue W178S PROKR2 reflected where this chemical binds to the receptor—that is, A457 may only affect conformation around its binding site. The discrimination by mutations at different amino acid positions for the functional restoration of PROKR2 may further contribute to our understanding of different fates in the secretory pathway and thereby provide additional insight into disease-causing GPCR mutations.

Overall, in addition to contributing to a fundamental understanding of the different ways that cellular quality control can be achieved, our findings also suggest more avenues of therapeutic intervention for disease-causing mutations in GPCRs.

Materials and Methods

Cell Culture, Transfection, and siRNA Knockdown. HEK293T, COS-7, and HeLa cells were maintained in Dulbecco's modified Eagle's medium supplemented with 10% fetal bovine serum and antibiotics. For the generation and maintenance of stable cell lines, neomycin and geneticin were added to the cell culture medium. Transfections of plasmids or siRNA were performed using Lipofectamine 2000 or Lipofectamine RNAiMAX, respectively, following the manufacturer's instructions (Invitrogen). For experiments in which siRNA and

plasmid DNA were both transfected, siRNA transfection was performed first followed by plasmid transfection. ARFGAP1 (L-013321-02), KDELR1 (L-019136-01), RER1 (L-0117170-01) ON-TARGETplus Human SMARTpool siRNAs and RER1 (L-0117170-11) and customized siRNAs for HRD1 (5'-AAGGUGAUGGGCAAGGU GUUC) and gp78 (5'-AAGACGGAUUAAGUACUUUU) were purchased from Dharmacon. Scrambled siRNAs were used as negative controls (Invitrogen).

Plasmid Constructs. The majority of expression vectors were generated using Gateway cloning technology (Invitrogen). Briefly, complementary DNA (cDNA) was amplified using PCR and then subcloned into the pENTR-D/TOPO vector. Each cDNA in the TOPO vector was recombined into the pcDNA expression vector, which contained various N-terminal or C-terminal tags (Invitrogen). The procedures were followed according to the manufacturer's descriptions and modified as previously described (54). pcDNA expression vectors containing N or C terminus 3xFLAG-3xHA (3F3H) or C terminus 3xHA were used in these studies. Each PCR product encoding a GPCR conjugated with KKTN sequences at the C terminus was amplified from pcDNA-GPCR-3F3H constructs using cloning primers listed in *SI Appendix, Table S2* and then was inserted into the *KpnI* and *XbaI* restriction sites of the pcDNA-PROKR2-GFP plasmid. The expression plasmids for FLAG-tagged gp78 and His/Myc-tagged HRD1 were kindly provided by Yihong Ye (National Institute of Diabetes and Digestive and Kidney Diseases, NIH, Bethesda, MD) (55). All mutations were generated by site-directed mutagenesis (QuikChange II Site-Directed Mutagenesis Kit; Agilent) using primers listed in *SI Appendix, Table S2*.

Antibodies and Reagents. The antibodies used for immunoblotting, immunoprecipitation, and immunostaining are listed in *SI Appendix, Table S3*. Additional detailed methods and reagents are provided in *SI Appendix*.

Immunoblotting and Immunoprecipitation. The cells were lysed with M-PER mammalian protein extraction reagent (Thermo Scientific) containing protease inhibitor mixtures (Roche). The extracted proteins were mixed with 5x sodium dodecyl sulfate-polyacrylamide gel electrophoresis (SDS-PAGE) sample buffer for 1 h at room temperature. The proteins were separated on SDS-PAGE gels and then transferred to nitrocellulose membranes. The bands were detected using the Chemidoc imaging system (Bio-Rad), and the signal intensity was quantified by ImageJ software.

For immunoprecipitation, cells were lysed using M-PER buffer. Additional detailed methods are provided in *SI Appendix*.

Mass Spectrometry and Bioinformatics. For the immunoprecipitation experiments, the total protein from stable cell lines expressing WT PROKR2 or P290S PROKR2 or from stable cell line expressing the pcDNA vector as a control was harvested from 12 100-mm plates. Additional detailed methods are provided in *SI Appendix*.

For the protein enrichment analysis of interacting proteins, GO analysis was performed using the PANTHER database (released version 2015-08-06; <http://www.pantherdb.org/>) (56).

Egr1-Luciferase Assay. An Egr1-luciferase assay was used to measure PROKR2 activity and was performed as previously described (57). Additional detailed methods are provided in *SI Appendix*.

Real-Time qPCR. Total RNA was isolated from the cells using the RNeasy Mini Kit according to the manufacturer's instructions (Qiagen). The primers used in qRT-PCR are listed in *SI Appendix, Table S2*.

Additional detailed materials and methods are provided in the online *SI Appendix*.

Data Availability. All study data are included in the article and/or supporting information.

ACKNOWLEDGMENTS. This work was supported by grants from the NIH to U.B.K. (U54 HD028138, R01/R37 HD019938, and R01 HD082314) and to V.W.H. (R37GM058615), and by grants from the National Research Foundation of Korea to S.-Y.P. (NRF-2020R1C1C1008823 and NRF-2017R1A5A1015366).

1. A. S. Hauser, M. M. Attwood, M. Rask-Andersen, H. B. Schiöth, D. E. Gloriam, Trends in GPCR drug discovery: New agents, targets and indications. *Nat. Rev. Drug Discov.* **16**, 829–842 (2017).
2. J. P. Overington, B. Al-Lazikani, A. L. Hopkins, How many drug targets are there? *Nat. Rev. Drug Discov.* **5**, 993–996 (2006).
3. K. L. Pierce, R. T. Premont, R. J. Lefkowitz, Seven-transmembrane receptors. *Nat. Rev. Mol. Cell Biol.* **3**, 639–650 (2002).
4. G. Vassart, S. Costagliola, G protein-coupled receptors: Mutations and endocrine diseases. *Nat. Rev. Endocrinol.* **7**, 362–372 (2011).

5. R. Balasubramanian *et al.*, Human GnRH deficiency: A unique disease model to unravel the ontogeny of GnRH neurons. *Neuroendocrinology* **92**, 81–99 (2010).
6. S. D. Noel, U. B. Kaiser, G protein-coupled receptors involved in GnRH regulation: Molecular insights from human disease. *Mol. Cell. Endocrinol.* **346**, 91–101 (2011).
7. M. Y. Cheng *et al.*, Prokineticin 2 transmits the behavioural circadian rhythm of the suprachiasmatic nucleus. *Nature* **417**, 405–410 (2002).
8. C. Dodé *et al.*, Kallmann syndrome: Mutations in the genes encoding prokineticin-2 and prokineticin receptor-2. *PLoS Genet.* **2**, e175 (2006).

9. M. Li, C. M. Bullock, D. J. Knauer, F. J. Ehler, Q. Y. Zhou, Identification of two prokineticin cDNAs: Recombinant proteins potentially contract gastrointestinal smooth muscle. *Mol. Pharmacol.* **59**, 692–698 (2001).
10. S. Matsumoto *et al.*, Abnormal development of the olfactory bulb and reproductive system in mice lacking prokineticin receptor PKR2. *Proc. Natl. Acad. Sci. U.S.A.* **103**, 4140–4145 (2006).
11. N. Pitteloud *et al.*, Loss-of-function mutation in the prokineticin 2 gene causes Kallmann syndrome and normosmic idiopathic hypogonadotropic hypogonadism. *Proc. Natl. Acad. Sci. U.S.A.* **104**, 17447–17452 (2007).
12. H. M. Prosser, A. Bradley, M. A. Caldwell, Olfactory bulb hypoplasia in Prokr2 null mice stems from defective neuronal progenitor migration and differentiation. *Eur. J. Neurosci.* **26**, 3339–3344 (2007).
13. H. Schweitz, P. Pacaud, S. Diochot, D. Moinier, M. Lazdunski, MIT(1), a black mamba toxin with a new and highly potent activity on intestinal contraction. *FEBS Lett.* **461**, 183–188 (1999).
14. C. Martin *et al.*, The role of the prokineticin 2 pathway in human reproduction: Evidence from the study of human and murine gene mutations. *Endocr. Rev.* **32**, 225–246 (2011).
15. P. M. Conn, A. Ulloa-Aguirre, J. Ito, J. A. Janovick, G protein-coupled receptor trafficking in health and disease: Lessons learned to prepare for therapeutic mutant rescue in vivo. *Pharmacol. Rev.* **59**, 225–250 (2007).
16. L. W. Cole *et al.*, Mutations in prokineticin 2 and prokineticin receptor 2 genes in human gonadotrophin-releasing hormone deficiency: Molecular genetics and clinical spectrum. *J. Clin. Endocrinol. Metab.* **93**, 3551–3559 (2008).
17. C. Monnier *et al.*, PROKR2 missense mutations associated with Kallmann syndrome impair receptor signalling activity. *Hum. Mol. Genet.* **18**, 75–81 (2009).
18. J. Sarfati *et al.*, A comparative phenotypic study of Kallmann syndrome patients carrying monoallelic and biallelic mutations in the prokineticin 2 or prokineticin receptor 2 genes. *J. Clin. Endocrinol. Metab.* **95**, 659–669 (2010).
19. O. Sbai *et al.*, Biased signaling through G-protein-coupled PROKR2 receptors harboring missense mutations. *FASEB J.* **28**, 3734–3744 (2014).
20. J. A. Janovick *et al.*, Restoration of testis function in hypogonadotropic hypogonadal mice harboring a misfolded GnRHR mutant by pharmacoperone drug therapy. *Proc. Natl. Acad. Sci. U.S.A.* **110**, 21030–21035 (2013).
21. J. P. Morello *et al.*, Pharmacological chaperones rescue cell-surface expression and function of misfolded V2 vasopressin receptor mutants. *J. Clin. Invest.* **105**, 887–895 (2000).
22. C. L. Newton *et al.*, Rescue of expression and signaling of human luteinizing hormone G protein-coupled receptor mutants with an allosterically binding small-molecule agonist. *Proc. Natl. Acad. Sci. U.S.A.* **108**, 7172–7176 (2011).
23. D. N. Chen, Y. T. Ma, H. Liu, Q. Y. Zhou, J. D. Li, Functional rescue of Kallmann syndrome-associated prokineticin receptor 2 (PKR2) mutants deficient in trafficking. *J. Biol. Chem.* **289**, 15518–15526 (2014).
24. J. Fan, S. J. Perry, Y. Gao, D. A. Schwarz, R. A. Maki, A point mutation in the human melanin concentrating hormone receptor 1 reveals an important domain for cellular trafficking. *Mol. Endocrinol.* **19**, 2579–2590 (2005).
25. D. Mizrahi, D. L. Segaloff, Intracellularly located misfolded glycoprotein hormone receptors associate with different chaperone proteins than their cognate wild-type receptors. *Mol. Endocrinol.* **18**, 1768–1777 (2004).
26. J. P. Morello *et al.*, Association of calnexin with wild type and mutant AVPR2 that causes nephrogenic diabetes insipidus. *Biochemistry* **40**, 6766–6775 (2001).
27. F. U. Hartl, Protein misfolding diseases. *Annu. Rev. Biochem.* **86**, 21–26 (2017).
28. A. Rivero-Müller *et al.*, A novel inactivating mutation of the LH/chorionic gonadotrophin receptor with impaired membrane trafficking leading to Leydig cell hypoplasia type 1. *Eur. J. Endocrinol.* **172**, K27–K36 (2015).
29. M. Wang, R. J. Kaufman, Protein misfolding in the endoplasmic reticulum as a conduit to human disease. *Nature* **529**, 326–335 (2016).
30. S. A. Houck *et al.*, Quality control autophagy degrades soluble ERAD-resistant conformers of the misfolded membrane protein GnRHR. *Mol. Cell* **54**, 166–179 (2014).
31. S. Pan, X. Cheng, R. N. Sifers, Golgi-situated endoplasmic reticulum α -1, 2-mannosidase contributes to the retrieval of ERAD substrates through a direct interaction with γ -COP. *Mol. Biol. Cell* **24**, 1111–1121 (2013).
32. K. Yamamoto *et al.*, The KDEL receptor mediates a retrieval mechanism that contributes to quality control at the endoplasmic reticulum. *EMBO J.* **20**, 3082–3091 (2001).
33. P. Satpute-Krishnan *et al.*, ER stress-induced clearance of misfolded GPI-anchored proteins via the secretory pathway. *Cell* **158**, 522–533 (2014).
34. B. C. Cross *et al.*, The molecular basis for selective inhibition of unconventional mRNA splicing by an IRE1-binding small molecule. *Proc. Natl. Acad. Sci. U.S.A.* **109**, E869–E878 (2012).
35. M. Schröder, R. J. Kaufman, The mammalian unfolded protein response. *Annu. Rev. Biochem.* **74**, 739–789 (2005).
36. C. Hetz, F. R. Papa, The unfolded protein response and cell fate control. *Mol. Cell* **69**, 169–181 (2018).
37. Y. Liu, A. Chang, Heat shock response relieves ER stress. *EMBO J.* **27**, 1049–1059 (2008).
38. M. R. Jackson, T. Nilsson, P. A. Peterson, Identification of a consensus motif for retention of transmembrane proteins in the endoplasmic reticulum. *EMBO J.* **9**, 3153–3162 (1990).
39. M. C. Lee, E. A. Miller, J. Goldberg, L. Orci, R. Schekman, Bi-directional protein transport between the ER and Golgi. *Annu. Rev. Cell Dev. Biol.* **20**, 87–123 (2004).
40. M. L. Styers, A. K. O'Connor, R. Grabski, E. Cormet-Boyaka, E. Sztul, Depletion of beta-COP reveals a role for COP-I in compartmentalization of secretory compartments and in biosynthetic transport of caveolin-1. *Am. J. Physiol. Cell Physiol.* **294**, C1485–C1498 (2008).
41. M. Bai *et al.*, ARFGAP1 promotes AP-2-dependent endocytosis. *Nat. Cell Biol.* **13**, 559–567 (2011).
42. M. G. Waters, T. Serafini, J. E. Rothman, 'Coatmer': A cytosolic protein complex containing subunits of non-clathrin-coated Golgi transport vesicles. *Nature* **349**, 248–251 (1991).
43. F. Letourneur *et al.*, Coatmer is essential for retrieval of dilysine-tagged proteins to the endoplasmic reticulum. *Cell* **79**, 1199–1207 (1994).
44. H. R. Pelham, The Florey Lecture, 1992. The secretion of proteins by cells. *Proc. Biol. Sci.* **250**, 1–10 (1992).
45. K. Sato, S. Nishikawa, A. Nakano, Membrane protein retrieval from the Golgi apparatus to the endoplasmic reticulum (ER): Characterization of the RER1 gene product as a component involved in ER localization of Sec12p. *Mol. Biol. Cell* **6**, 1459–1477 (1995).
46. K. Sato, M. Sato, A. Nakano, Rer1p as common machinery for the endoplasmic reticulum localization of membrane proteins. *Proc. Natl. Acad. Sci. U.S.A.* **94**, 9693–9698 (1997).
47. K. Sato, M. Sato, A. Nakano, Rer1p, a retrieval receptor for endoplasmic reticulum membrane proteins, is dynamically localized to the Golgi apparatus by coatmer. *J. Cell Biol.* **152**, 935–944 (2001).
48. M. Sato, K. Sato, A. Nakano, Endoplasmic reticulum localization of Sec12p is achieved by two mechanisms: Rer1p-dependent retrieval that requires the transmembrane domain and Rer1p-independent retention that involves the cytoplasmic domain. *J. Cell Biol.* **134**, 279–293 (1996).
49. L. Achour, C. Labbé-Jullié, M. G. Scott, S. Marullo, An escort for GPCRs: Implications for regulation of receptor density at the cell surface. *Trends Pharmacol. Sci.* **29**, 528–535 (2008).
50. M. T. Drake, S. K. Shenoy, R. J. Lefkowitz, Trafficking of G protein-coupled receptors. *Circ. Res.* **99**, 570–582 (2006).
51. S. R. Caldwell, K. J. Hill, A. A. Cooper, Degradation of endoplasmic reticulum (ER) quality control substrates requires transport between the ER and Golgi. *J. Biol. Chem.* **276**, 23296–23303 (2001).
52. C. Hammond, A. Helenius, Quality control in the secretory pathway: Retention of a misfolded viral membrane glycoprotein involves cycling between the ER, intermediate compartment, and Golgi apparatus. *J. Cell Biol.* **126**, 41–52 (1994).
53. S. Vashist *et al.*, Distinct retrieval and retention mechanisms are required for the quality control of endoplasmic reticulum protein folding. *J. Cell Biol.* **155**, 355–368 (2001).
54. Y. B. Song, C. O. Park, J. Y. Jeong, W. K. Huh, Monitoring G protein-coupled receptor activation using an adenovirus-based β -arrestin bimolecular fluorescence complementation assay. *Anal. Biochem.* **449**, 32–41 (2014).
55. Y. Liu *et al.*, USP13 antagonizes gp78 to maintain functionality of a chaperone in ER-associated degradation. *eLife* **3**, e01369 (2014).
56. H. Mi, S. Poudel, A. Muruganujan, J. T. Casagrande, P. D. Thomas, PANTHER version 10: Expanded protein families and functions, and analysis tools. *Nucleic Acids Res.* **44**, D336–D342 (2016).
57. A. P. Abreu *et al.*, Evidence of the importance of the first intracellular loop of prokineticin receptor 2 in receptor function. *Mol. Endocrinol.* **26**, 1417–1427 (2012).